Oscillating Taylor bubble during the emptying of a partially filled water bottle

Olivier Praud ⬤,[*] Cyril Vettorello ⬤, and Véronique Roig ⬤

Institut de Mécanique des Fluides de Toulouse, IMFT, Université de Toulouse-CNRS, 31400 Toulouse, France

The oscillatory behavior observed during the emptying of a vertical cylinder partially filled with water has been studied for large neck-to-bottle diameter ratios, d^*. For large apertures ($d^* > 0.8$), a Taylor bubble invades the cylinder from the bottom, and its rising speed exhibits periodic oscillations coupled to periodic motions of the free surface limiting the top air buffer initially present in the bottle. We introduce an elementary model where the vertical oscillation of the free surface is represented by a variable mass oscillator exciting the oscillatory dynamics of the Taylor bubble. In this system, the top-air buffer acts as a spring, whose stiffness is related to its compressibility. The variable mass is the mass of the liquid in the cylinder that decreases as the Taylor bubble progresses during the emptying. The motion of the bubble is solved assuming that the unsteady flow generated by the free-surface motion is potential in the vicinity of the apex of the bubble. A comparison with experimental results obtained at the laboratory shows that the model agrees well with the data if it takes into account dissipation. This study shows that a viscous damping, proportional to the velocity, with a constant damping coefficient is able to accurately represent the dissipative processes such as the effect of viscous Stokes boundary layers at the walls.

I. INTRODUCTION

Emptying a vertical bottle in an ambient medium creates a common gas-liquid gravity-driven flow. It is an unsteady two-phase flow where the liquid present in the bottle is evacuated intermittently from the neck located at the bottom of the reversed bottle. The flow is characterized by a periodic alternation of air inlet and liquid outlet through the neck. The mass of liquid inside the bottle decreases over time, and the top air buffer, initially present in the bottle and fed by the entry of gas, is submitted to compressibility effects. In the low viscosity and surface tension limits that we consider, various contrasted two-phase flow regimes can be observed, depending on the shape of the neck and on the ratio between the neck and the bottle diameters, d^*. For small and moderated openings, periodic detachment of isolated bubbles from the neck imposes regular air feeding of the top air buffer until the bottle is empty [1,2]. For large openings, the flow exhibits a different configuration that consists in a unique large air bubble that invades the bottle [3]. The case $d^* = 1$ corresponds to the configuration that has been commonly used to study the motion of Taylor bubbles in cylinders of large length-to-diameter ratios as in [4–6]. During emptying, the rear part of this Taylor bubble can be either attached to the neck for extreme apertures or fed by the swarm of coalescing bubbles expelled from the neck that follows the large bubble for less important apertures [3]. When the rear part of the bubble is attached to the neck and opened to the atmosphere, a periodic modulation of the outflows of liquid associated with periodic inflows of air is observed. In this case, any top air

buffer initially present remains a closed system until the large bubble crosses its limiting bottom interface.

In the literature, the first studies reported on emptying assessed the influence of the geometry—the bottle size, shape, and neck diameter—on the global emptying time [7–11]. General properties have appeared rapidly: (i) the liquid discharge rate remains constant throughout the emptying of the bottle; (ii) the slowly varying average pressure difference between the top air buffer and the ambient medium scales well with the hydrostatic head of the water column; (iii) the global emptying time depends on the bottle neck shape and diameter. Depending on the mentioned parameters, the oscillating alternation of gas and liquid flows at the neck may indeed vary a lot, thus exciting contrasted global oscillations of the flow that contribute to contrasted total emptying times. Considering bottles open at the bottom through a circular thin-walled hole, Clanet and Searby have provided a general scaling law relating the emptying time to the geometrical parameters in the low viscosity and surface tension limits [2]. This law is still valid for small to large apertures when the bottle is initially partially filled [3].

The oscillatory behavior of the flow was studied later for small apertures, in the regime where chains of isolated bubbles rise from the neck to the air top buffer [1,2]. Their periodic entries in the bottle induce oscillations of the top air buffer pressure. For such a regime, Tehrani *et al.* proposed a one-dimensional model for the emptying of a partially filled sealed tank through a single vertical long tube of small diameter ($d^* \lesssim 0.1$) [1]. They proposed to decompose any period of the oscillation into three parts, the first one being associated with the liquid down flow in the tube, the second one to the following bubble rise in the tube, and the final phase being associated with the tank repressurization. With this *a*

---
[*]olivier.praud@imft.fr

priori decomposition of the oscillation of the flow, and using one-dimensional two-phase flow models for each phase as in [12], they predicted an amplitude and a period of the oscillations that were in good agreement with their experimental observations. Later, Clanet and Searby introduced the elegant description of the flow as an equivalent mass-spring system where the compressibility of the top air buffer defines the stiffness of the spring, and the mass of liquid in the bottle defines the evolving mass of the system [2]. For a neck designed as a circular thin-walled hole, they noticed, however, that the resulting simple scaling law for the period deviates from experimental observations when the neck-to-bottle diameter ratio is small. They then developed a nonlinear model that better reproduces the observations.

The present study focuses on the oscillating behavior of the flow observed for very large apertures ($d^* \geqslant 0.8$) in a thin-walled neck where a Taylor bubble forms and propagates through the bottle. We will see that for this configuration, as the gas and liquid flows at the neck are continuous even if they are modulated periodically, a continuous model can be developed to predict the oscillations of the rising velocity of the bubble and of the position of the free surface limiting the top air buffer.

Oscillating Taylor bubbles rising in pipes filled with stagnant fluid have been reported in Ref. [13]. For an experiment with a top end of the pipe open to the atmosphere, in case of an abrupt change of air injection conditions, Pringle *et al.* observed that the Taylor bubble rose in an oscillatory manner. The length of the bubble oscillated with an amplitude and a period that decreased during the rise. They clearly related the oscillating period to the compressibility of the bubble, but the linear harmonic oscillator equation they introduced was not able to predict the attenuation of the amplitude. Later, Ambrose *et al.* simulated this flow numerically [14] and introduced a damping term in the oscillator equation representing the viscous dissipation in the Stokes boundary layers that developed in the liquid. Of course, this damping term did attenuate the motions, but data for comparison between numerical simulations and the oscillatory model were scarce and did not prove clearly that the rate of damping is a generic one. Explorations that can also bring ideas to understand the unsteady motion of the emptying of a bottle with a large aperture concern the motion of Taylor bubbles in vertical oscillating pipes. Brannock and Kubie's experiments have first shown that pipe oscillations lead to a decrease of the mean velocity of the bubble when the relative acceleration of the tube increases [15]. A physical model was then proposed in Ref. [6] that proved that an unsteady potential flow model is sufficient to reproduce this behavior. Later, experimental studies of Madani *et al.* provided interesting insights on the contrasted evolutions of mean and fluctuating velocities with the relative acceleration of the sinusoidal forcing [16,17]. Exploring larger relative accelerations as compared to [15], they have shown that above a critical acceleration, from which shape disturbances appear, the mean velocity may increase again when the relative acceleration increases. They have thus pointed out important Bond effects on the response of the bubble velocity to the pipe oscillation.

The present contribution concerns the modeling of the oscillatory behavior of the emptying of a bottle in the regime of large aperture. It has not been discussed up to now, as far as we know. In the following sections, the experimental means of the study are first presented, as well as preliminary observations useful to build the model. Then, a model built to predict the top air buffer pressure oscillations and the coupled bubble velocity oscillations is proposed. In a final section, the capacity of prediction of the model and its limits is discussed, including a comparison of the model's predictions with the experimental results.

II. EXPERIMENTAL SETUP AND MEASUREMENT TECHNIQUES

For the sake of clarity, we describe the device and measurement techniques that we used, even if this device and these techniques as well as the experimental protocol are similar to those employed by [18], while the present operating conditions are different.

A. Experimental setup

The experimental setup is depicted by Fig. 1. It consists of a Plexiglas™ cylinder with an inner diameter $D = 100$ mm, its total height being $L = 825$ mm. The cylinder is closed at its top end, while a central circular thin-walled hole with a diameter d can be opened at its bottom. The neck diameter can be varied from 20 mm to $d = 100$ mm for complete opening. Before a test, the cylinder is filled with tap water up to an altitude L_0 using a pump. The initial pressure at the top of the bottle is the atmospheric pressure, P_a, as filling is performed with an opened top valve v_{out}. The bottom tank is for water recovery and is open at atmospheric pressure. When filling is finished, both top valves v_{in} and v_{out} are closed. At time $t = 0$, the bottom gate mounted on hinges is actuated by
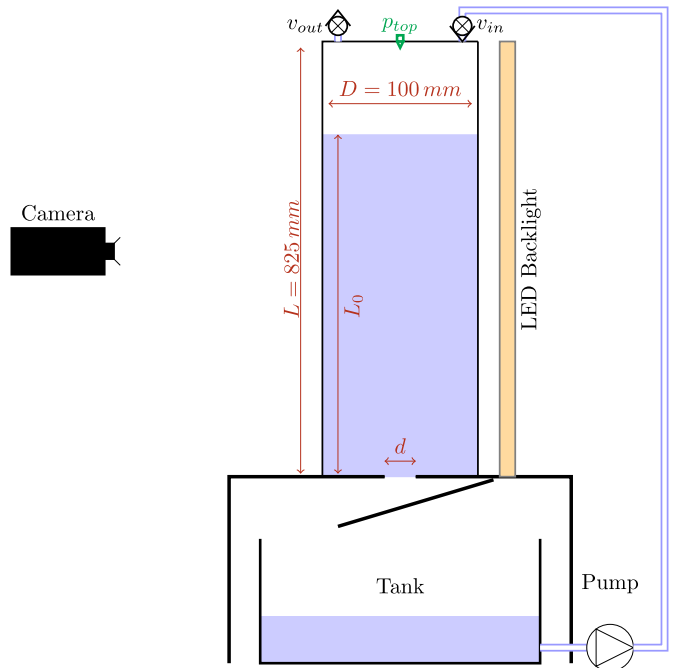

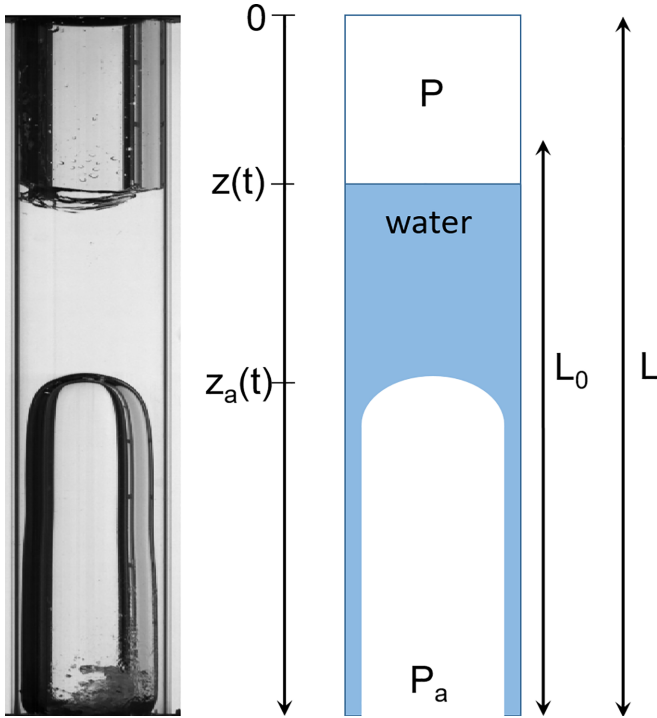FIG. 1. Schematic of the experimental setup and measurement means.

FIG. 2. Left: Visualization of the gas and liquid contents in the cylinder for a full opening ($d^* = 1$). For such a large opening, the rising gas entity takes the form of a Taylor bubble whose apex position is given by $z_a(t)$. For an initial filling level L_0, the free surface separating the top air buffer from the internal liquid region is located at position $z(t)$. Right: Simplified description of the system used to construct the mechanical model.

electromagnets that ensure a fast opening. Water then starts to flow out of the vessel in succession of liquid jets separated by entering large air bubbles at the neck.

In the present study, the normalized outlet diameter, $d^* = d/D$, and the initial filling ratio, $\mathcal{F} = L_0/L$, are varied in the ranges $0.8 \leqslant d^* \leqslant 1$ and $0.73 \leqslant \mathcal{F} \leqslant 0.97$, respectively. Focusing on large values of d^*, the present study will involve large bubbles formed at the neck that are unsteady but that differ from a periodic alternation of separated bubbles crossing the neck. Varying $\mathcal{F}$ allows us to discuss the impact of the compressibility of the upper air buffer on the dynamics. The density and kinematic viscosity of the water used in the experiments, performed at room temperature, are $\rho_l = 997 \text{ kg m}^{-3}$ and $\nu_l = 1 \times 10^{-6} \text{ m}^2 \text{ s}^{-1}$, respectively.

B. Measurement techniques

The air pressure at the center of the top end of the cylinder, P, is recorded with a pressure sensor (Keller, PR-23) at a sampling frequency $f_p = 1000$ Hz. Images of the emptying process are simultaneously recorded with a synchronized PCO™ Dimax camera with a full resolution of 2000×2000 pixels operated at a frequency $f_{\text{im}} = 200$ Hz. A LED panel provides the back-light that allows us to obtain typical images such as the Taylor bubble rising in the cylindrical tube presented on the left part of Fig. 2. The recorded images are postprocessed to extract the vertical position of the apex of this bubble as a function of time, $z_a(t)$. The camera resolution

is 0.5 mm/pix. We take the z-axis oriented vertically in the direction of gravity with the origin at the top of the cylinder.

III. PRELIMINARY EXPERIMENTAL OBSERVATIONS

General visual observations are reported to introduce the physics of the model developed to reproduce the dynamics of the oscillations of the flow. Once the gate is open, water starts to flow out of the cylinder, and air bubbles with a size of the order of d form at the neck. Depending on the neck diameter, a broad variety of two-phase flow configurations is observed [3], but for cases of large neck diameters ($d^* \geqslant 0.8$) investigated in the present study, a unique and large air bubble rapidly emerges and takes the form of a Taylor bubble as illustrated in Fig. 2. The emptying process then experiences two successive regimes: (i) before and (ii) after the bubble generated at the neck reaches the top of the liquid column and bursts at the free surface.

Along the first stage of the emptying process, air volume invades the cylinder, the length of the bubble increasing with time while its back face remains located at the bottom of the cylinder. Periodic oscillations of the radius of curvature of the bubble are observed at its rear neck and are associated with a pulsating outflow of liquid. For $d^* \geqslant 0.8$, the magnitude of this bubble radius modulation is, however, not sufficient to lead to a pinch off of the rear bubble interface, and the bubble remains always connected to the outside. During this stage, the free surface at the bottom of the upper air buffer layer—located at $z(t)$—as well as the large bubble apex—located at $z_a(t)$—present coupled oscillations. At time τ, the bubble reaches the upper free surface and becomes part of the top air buffer. Beyond this time, the liquid that was trapped in the film between the bubble and the tube falls under gravity, mixes with air, and forms a two-phase flow at the bottom of the tube. Then starts the second regime corresponding to the emptying of the gas-liquid mixture. This stage, that lasts until the complete drainage of liquid, is beyond the scope of this study. The duration of the first stage, on which this study focuses, is determined by the time τ required for the Taylor bubble to reach the free surface, which, in a first approximation, increases linearly with $\mathcal{F}$.

The typical time evolution of the apex position of the bubble $z_a(t)$, obtained by image processing, is displayed in Fig. 3(a) for $d^* = 0.9$ and $\mathcal{F} = 0.97$. In the very early stage after the gate opening, which corresponds to the time for the Taylor bubble to form, no data can be extracted for $z_a(t)$. But after this short transient, which lasts for approximately 0.1–0.2 s, the height of the apex increases almost linearly over time until the air bubble bursts at the upper free surface. A closer look to the vertical velocity of the bubble [Fig. 3(b)] reveals that the apex rise speed oscillates about a very slowly varying value with a characteristic period of the order of 0.1 s, much shorter than the bursting time (the order of magnitude of which is $\tau \sim 2.4$ s in this case). The slowly varying bubble rise speed decreases, in 0.5 s, from 0.4 ms^{-1} to a constant value equal to $U_b = 0.33$ ms^{-1}, which was found to be independent of d^*. This value agrees with the findings of Ref. [3], namely that the rise speed of gas spherical caps in a cylindrical tube, initially partially filled with water, is close to $0.34\sqrt{gD}$ for a large range of neck diameters up to $d^* = 0.7$. It is also
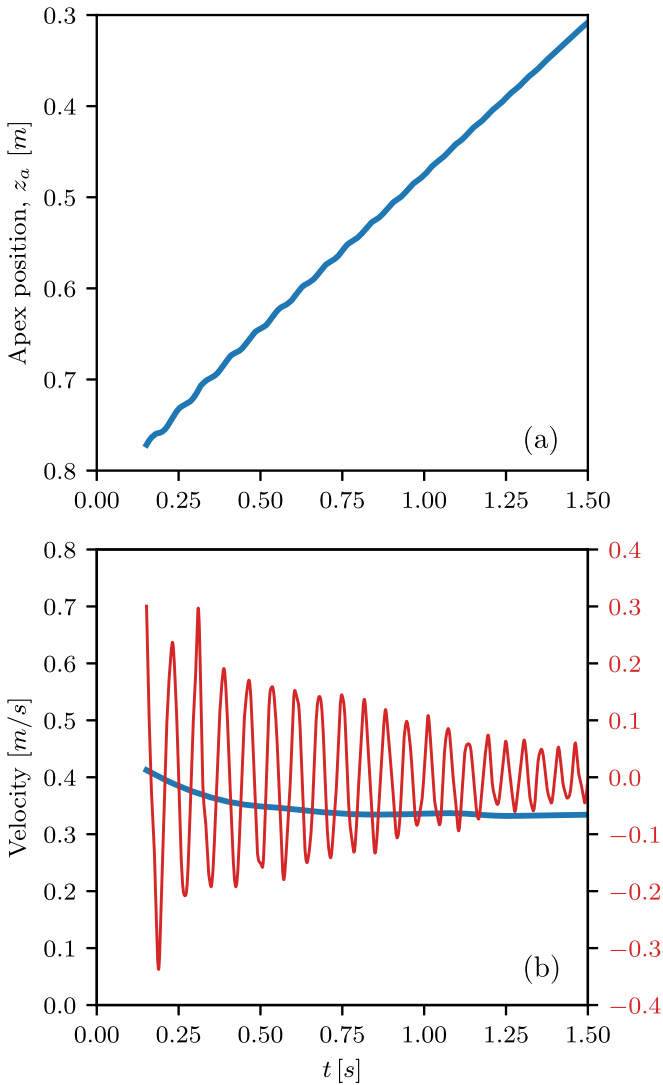
FIG. 3. (a) Measured positions of the apex of the bubble; (b) rise speed of the bubble decomposed into a slowly varying part (blue) and an oscillating part (red). $\mathcal{F} = 0.97$ and $d^* = 0.9$.

FIG. 4. Time evolution of the pressure in the top air buffer for $d^* = 0.9$ and $\mathcal{F} = 0.97$. For this case, the bubble reaches the free surface at time $\tau = 2.4$ s.

in close agreement with the well-known laws of motion of Taylor bubbles in long tubes provided by [4,5]. A moderate attenuation as compared to their predictions is observed, however, that may be related to the appearance of oscillations as in [15].

The time evolution of the pressure of the top air buffer along the emptying of a bottle is shown in Fig. 4. Starting from the atmospheric pressure P_a, the top air buffer pressure $P(t)$ immediately drops after the gate opening. The pressure drop is larger than the hydrostatic pressure variation corresponding to the height of the liquid column, $\rho_l g L \mathcal{F}$. Then as the bubble rises in the cylinder, the pressure of the top air buffer oscillates around a linearly increasing value $P_e(t)$ until it recovers its initial value P_a at the end of the emptying process. It is observed that the rising velocity of the bubble and the pressure oscillations are out of phase. Before the large bubble generated at the neck reaches the top of the liquid column (at $t = 2.4$ s for the case displayed in Fig. 4), the air buffer forms a closed gas volume with a constant mass.
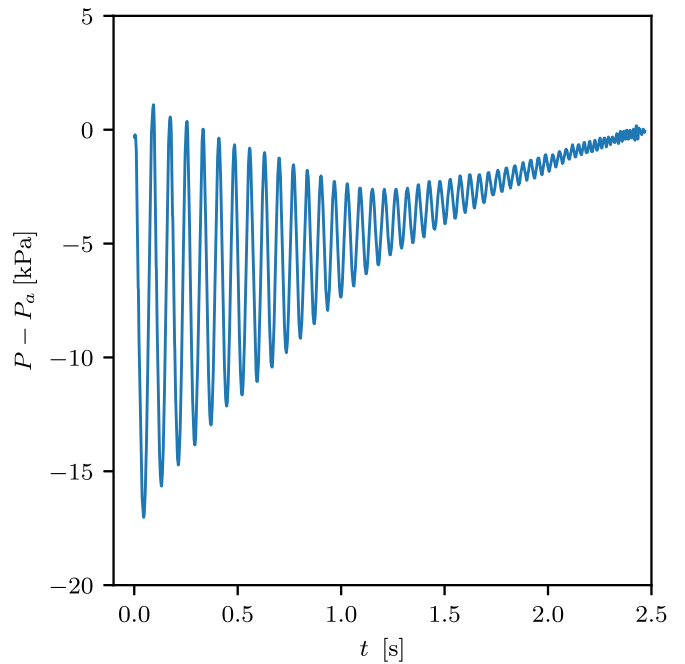
During this stage, the amplitude of the oscillations decreases over time at a rate that is found to depend essentially on $\mathcal{F}$ and barely on d^* as discussed in the following. Concurrently, the period of the oscillations decreases with time until the bubble bursts at the free surface. Just at this time, a sudden change in the pressure signal is observed which is characterized by an abrupt increase of the period of oscillations associated with the sudden increase of the volume of the top air buffer. Then the second regime of the emptying starts.

Experimental observations also reveal that, as the Taylor bubble rises in the water column, and until it reaches the upper free surface, the position of the free surface oscillates around a constant position z_e. The volume of the bubble which increases linearly with time compensates for the volume of liquid that exits from the bottle, leaving the position of the free surface unchanged. The amplitude of oscillation of the position of the free surface around z_e is compared to the amplitude of oscillation of the apex position around its slowly moving part in Fig. 5. It appears that the apex position exhibits greater oscillation amplitude as compared to the free-surface position one. For example, shortly after the gate opening ($t = 0.2$ s), the amplitude for the apex position is ~15 mm, while it is only ~10 mm for the free-surface position. Both amplitudes gradually decrease over time, reaching approximately half of their initial values by $t = 1$ s. In addition, it should be noted that the apex and the free-surface positions do not oscillate in phase. Both observations suggest that the oscillations of the apex position are not just mimicking the displacement of the free surface, and a more precise interaction has to be considered to model this behavior. A similar comparison was carried out for the other sets of parameters investigated in the study, leading to the same conclusion. Figure 5 also shows that the free surface and the pressure in the top air buffer
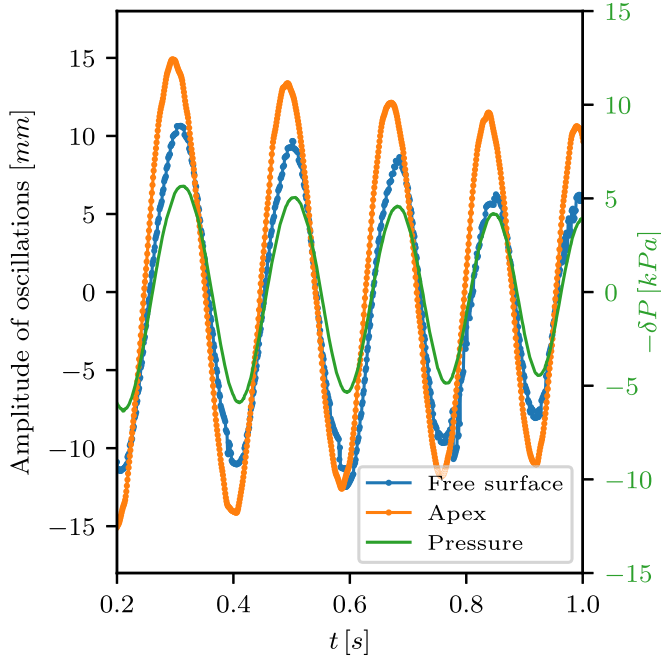
FIG. 5. Time evolution (for $0.2 \leqslant t \leqslant 1$ s) of the amplitude of oscillation of the free-surface position around $z_e = 236$ mm (orange), of the apex position around the slowly moving part (blue), and of the pressure in the top air buffer (green). $d^* = 0.9$ and $\mathcal{F} = 0.73$.

oscillate in phase, in agreement with previous observation [3] and consistent with the idea that the air buffer behaves as a closed thermodynamic system with a constant mass.

When the apex of the bubble reaches the region very close to the free surface, coupling between both interface motions becomes very complex: the free surface may slosh with large inclinations so that the approaching Taylor bubble may lose its axisymmetry, adapting its curvature at the apex, which affects its slowly varying speed. Also, even if its level stays horizontal on average, the free surface may sometimes present a huge deformation associated with an expulsion of liquid consisting in an ascending central thin jet that finally breaks into droplets that may entrain air bubbles underwater when they finally fall. Such an event is more frequently observed for moderate initial filling ($\mathcal{F} = 0.73$). The transient of this final approach of both interfaces, which involves fine scale and very rapid pinch-off mechanisms, is, however, beyond the scope of the present model. Experiments were performed for smaller initial filling ($\mathcal{F} < 0.5$). They are also beyond the scope of the present model and are not reported in this contribution. In this case, the forming bubble may exhibit several lobes or may grow off center with respect to the tube axis. In addition, because of its initial proximity, the bubble rapidly interacts with the upper free surface leading to large interface deformations.

IV. MODEL

A. Model for the pressure oscillations

As already observed and described by [6,18], the pressure oscillations find their origin in the alternation of air entrance and liquid ejection events at the neck of the cylinder. We propose here a mechanical model specifically adapted for very

large openings ($d^* \gtrsim 0.8$) that predicts the pressure evolution in the top air buffer during the first stage of the emptying process ($t \leqslant \tau$).

We consider a situation depicted in Fig. 2 (right) where a large bubble rises in a cylindrical tube of length L initially filled with water of density ρ_l up to an altitude L_0. We denote as $P(t)$ and $z(t)$, respectively, the instantaneous pressure of the top air buffer and the position of the upper free surface. The two-phase column located below the free surface is considered as an equivalent liquid of height $(L - z)$ and of effective density evolving with time $\rho(t)$, while the bubble propagates in the liquid. The rise speed of the bubble, U_b, being in a first approximation constant, the effective density is taken as decreasing linearly with time,

$$\rho(t) = \rho_l(1 - t/\tau), \tag{1}$$

where $\tau = L_0/U_b$ is the time when the bubble reaches the free surface and becomes part of the top air buffer. The mass of the thin liquid film, present between the bubble and the vertical wall of the cylinder, is neglected in this approximation, and the Taylor bubble is assumed as being schematically a cylinder. Experimental observations revealed that, as the bubble rises, the pressure of the top air buffer oscillates around a slowly increasing value $P_e(t)$ while the free surface position also oscillates around a constant position z_e. Let us now write

$$P(t) = P_e(t) + \delta p(t), \quad z(t) = z_e + \delta z(t), \tag{2}$$

where $\delta p(t)$ and $\delta z(t)$ are small oscillations around their equilibrium counterparts. Considering a polytropic transformation of a perfect gas with a polytropic exponent α, pressure and upper free-surface position fluctuations are related by

$$\delta p = -\alpha P_e \delta z/z_e. \tag{3}$$

Assuming that the effective liquid column is subjected to pressure, gravity forces, and to a dissipative force denoted $F_f \pi D^2/4$, we write from the momentum equation

$$(L - z)\rho \frac{d^2z}{dt^2} = (L - z)\rho g + P - P_a + F_f, \tag{4}$$

where P_a is the ambient pressure.

The damping term is essential for the prediction of the oscillations, and its possible physical origins are discussed in the last section of the paper. It is considered proportional to the velocity of the fluid column, $F_f = -\beta dz/dt$, where the constant of proportionality β may depend on the neck diameter, the initial filling height, and the physical properties of the fluid. This yields, at the leading and first order,

$$P_e = P_a[1 - \eta(1 - z_e^*)], \tag{5}$$

$$\rho(t)\ddot{\delta z} + b\dot{\delta z} + a\delta z = 0, \tag{6}$$

with

$$a = \frac{P_a}{L^2} \frac{1}{(1 - z_e^*)} \left[\eta + \alpha \frac{1 - \eta(1 - z_e^*)}{z_e^*} \right], \tag{7}$$

$$b = \frac{\beta}{L} \frac{1}{(1 - z_e^*)}, \tag{8}$$

$\eta = \rho g L/P_a$, and $z_e^* = z_e/L$. In our study, η is a small constant with a maximum value of 0.08 obtained at

$t = 0$. The expression (7) then reduces to the constant value $a = \alpha P_a / [L^2 z_e^*(1 - z_e^*)]$.

Equation (5) specifies that the slowly varying component of the top air buffer pressure corresponds to the instantaneous hydrostatic equilibrium associated with the weight of the liquid column. As the bubble rises, $P_e(t)$ increases linearly with time until it reaches the ambient pressure when the bubble arrives at the free surface. Equation (6) is the equation of motion of a one-dimensional damped oscillator with time-varying mass. For a constant effective density ($\rho = \rho_l$) and omitting the damping term ($\beta = 0$), we retrieve the equations derived by [6].

For this classical mechanical problem, the time variation of the amplitude $A(t)$ and period $T(t)$ of the oscillations can be approximated by

$$A(t) = A_0\left(1 - \frac{t}{\tau}\right)^{\gamma}, \quad T^2(t) = 4\pi^2 \rho(t)/a, \quad (9)$$

with $\gamma = 1/4 + b\tau/2\rho_l$, and A_0 is the initial amplitude [19]. The ratio $b\tau/2\rho_l$ can be interpreted as the ratio of the mechanical energy loss by friction and the potential energy loss due to the decreases of the mass of the water column.

B. Model for the apex velocity oscillations

For large values of the neck diameter ($d^* \geqslant 0.8$), the rising gas entity takes the form of a Taylor bubble, and experimental measurements have shown that the apex rise speed is not constant but oscillates around a mean value. This unsteady behavior involves a coupling between the large bubble and the free surface whose position vertically oscillates with time. In this section, we develop a model that describes the motion of a large bubble rising through an unsteady axial flow imposed by the motion of the upper free surface. We assume, as is done in a lot of studies [4–6,20,21], that the flow around the nose of the rising bubble can be treated as that of an inviscid liquid, and, since the fluid is initially at rest, the flow is considered potential along time. Neglecting the viscosity is justified by the large value of the bubble Reynolds number, $U_b D/\nu_l \sim 3 \times 10^4$, which ensures that the boundary layer at the surface of the bubble remains very thin.

It is also assumed that, far in front of the bubble, the liquid velocity profile is uniform with a value equal to the upper free-surface velocity U_{fs}. This is justified by the large value of the Womersley number, which compares the cylinder radius R to the Stokes boundary layer thickness $\delta_{St} = (\nu_l/\omega)^{1/2}$ with $\omega = 2\pi/T$, and T is the period of oscillation of the position of the free surface. In our experiments, T is always lower than 0.2 s, which yields $\mathrm{Wo} = R\sqrt{2\pi/T\nu_l} \geqslant 300$.

In addition, buoyant forces dominate surface tension ones. In fact, the Eotvos number calculated with $\sigma = 0.072 \, \mathrm{N\,m^{-1}}$ for the water-air surface tension, $\mathrm{Eo} = \rho_l g D^2/\sigma \sim 1500$, is large enough to consider, in agreement with [22], that the effect of surface tension can be neglected in the description of the propagation of a Taylor bubble in the condition of our experiments.

We take a frame of reference with the origin at the position of the bubble nose (apex), the z axis oriented vertically downward, and we denote r the radial coordinate. In this frame of

reference, the velocity potential Φ satisfies the Laplace equation ($\Delta \Phi = 0$ and $\boldsymbol{u} = \nabla \Phi$) with the appropriate boundary conditions, which are (i) the normal component of the velocity is zero at the wall, $u_r(z, r = R) = 0$; (ii) the velocity at the apex it null, $\boldsymbol{u}(0, 0) = \boldsymbol{0}$; and (iii) the axial component of the velocity far ahead from the bubble is $u_z(z \to -\infty, r) = U_b + U_{fs}$. In this model, only one term of the infinite series expansion for the velocity potential $\phi(z, r, t)$ is retained. That yields

$$\phi(z, r, t) = \frac{U_b(t) + U_{fs}(t)}{k}(kz - J_0(kr)e^{kz}), \quad (10)$$

where J_0 is the Bessel function of order 0. The value of k comes from the condition of zero velocity at the wall. It is given by $kR \simeq 3.8317$, which is equal to the first zero of the Bessel function J_1. The rise speed $U_b(t)$ is then obtained by matching a dynamical condition at the interface, as explained hereafter.

In the non-Galilean frame of reference moving with the apex of the bubble, the motion of the fluid satisfies the Euler equation

$$\frac{\partial \boldsymbol{u}}{\partial t} + (\boldsymbol{u} \cdot \nabla)\boldsymbol{u} = \frac{1}{\rho}\nabla P + \boldsymbol{g} + \frac{dU_b}{dt}. \quad (11)$$

Neglecting surface tension and hydrostatic effects in the gas, we may take the pressure uniform within the bubble. Integrating Eq. (11) along the bubble surface from the stagnation point to a distance z from the apex, one obtains the condition for the fluid velocity at the surface of the bubble,

$$\frac{u^2}{2} = \left(g + \frac{dU_b}{dt}\right)z + \left.\frac{\partial \phi}{\partial t}\right|_0 - \left.\frac{\partial \phi}{\partial t}\right|_z. \quad (12)$$

Since Eq. (10) is only an approximation for the velocity potential, the condition Eq. (12) cannot be satisfied at any point of the surface for a single U_b. However, substitution of the expression of u^2 obtained from the velocity potential Eq. (10) in the region on the apex ($r, z \ll 1$) yields the differential equation

$$\frac{dU_b}{dt} + kU_b^2 + 2kU_b U_{fs} = g - kU_{fs}^2 - 2\frac{dU_{fs}}{dt}. \quad (13)$$

For a steady free surface, Eq. (13) reduces to the expression derived by [23] for the bubble rise speed: $U_b = \sqrt{g/k} \simeq 0.51\sqrt{gR}$, where R is the cylinder radius. This result is consistent, but slightly higher than reported experimental results [4,5]. When the position of the free surface is unsteady, this differential equation is the one that couples the ascending motion of the bubble to the velocity of the free surface. Let us now propose that

$$U_b = U_{b,0} + u_b, \quad U_{fs} = U_{fs,0} + u_{fs}, \quad (14)$$

where $U_{b,0}$ is the slow varying velocity of the bubble assimilated to the constant value $\sqrt{g/k}$, $U_{fs,0}$ is equal to zero for $t < \tau$, and u_b and u_{fs} are the amplitudes of the small oscillations around their equilibrium counterparts. Then, separating the oscillating part from the slowly varying part, we obtain, at the first order,

$$\frac{du_b}{dt} + 2kU_{b,0}(u_b + u_{fs}) + 2\frac{du_{fs}}{dt} = 0. \quad (15)$$
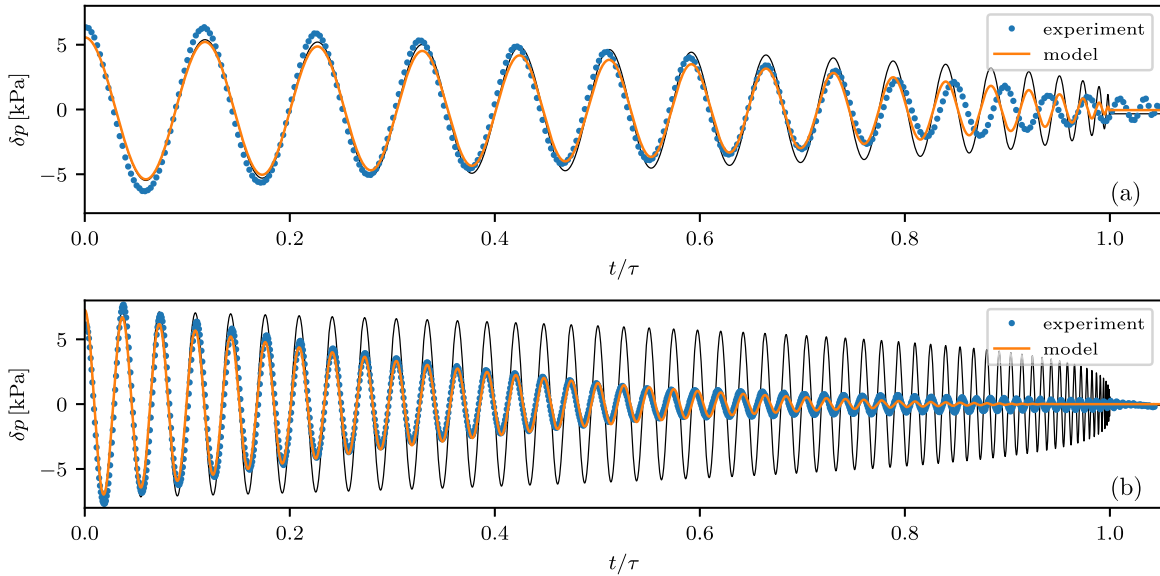
FIG. 6. Comparison of the time evolution of the pressure fluctuations between the prediction of the model and the experimental data for a full opening ($d^* = 1$) and two different initial filling ratios (a) $\mathcal{F} = 0.73$ and (b) $\mathcal{F} = 0.97$. The parameters (α, β) correspond to best-fitting values and are $(1.18, 170 \text{ N m}^{-3} \text{ s})$ for $\mathcal{F} = 0.73$ and $(1.14, 1250 \text{ N m}^{-3} \text{ s})$ for $\mathcal{F} = 0.97$. (Black thin lines are the predictions of the model when $\beta = 0$.)

The velocity of the upper free surface being given by the solution of Eq. (6) ($u_{\text{fs}} = \dot{\delta z}$), the rise speed of the apex of the bubble is then obtained by integration of Eq. (15).

To compare the prediction of the model with the experimental data, Eqs. (6) and (15) are numerically integrated. The initial conditions are chosen to match the experimental configurations. At $t = 0$ the pressure of the top air buffer is equal to the ambient pressure and thus larger than P_e. The upper free surface is initially at rest [$\delta z(0) = 0$] and its position $z_0 = L - L_0$ is above the equilibrium position, which is given by $z_e/z_0 = (1 - \eta\mathcal{F})^{-1/\alpha}$. We therefore have $\delta z(0) = z_0 - z_e$ and $u_b(0) = 0$.

For each experimental case, we integrate Eq. (6) to compute the time evolution of the oscillation of the free-surface position around its equilibrium altitude. We then deduce the pressure fluctuations through Eq. (3). The best-fitting parameters (α, β) minimize the sum of the squares of the errors with the experimentally measured pressure fluctuations. Integration of Eq. (15) using these best-fitting parameters (α, β) then provides the time evolution of the oscillations of the apex rise speed.

V. RESULTS AND DISCUSSION

A. Pressure oscillations model versus experiments

When measuring the pressure in the top air buffer, we found that the initial filling ratio $\mathcal{F}$ related to the magnitude of the initial difference from the hydrostatic pressure may change the amplitude and the period of the resulting pressure oscillations significantly. This is well illustrated in Fig. 6, where the measured pressure fluctuations for a full opening ($d^* = 1$) and two different initial filling ratios, $\mathcal{F} = 0.73$ and 0.97, are reported. The initial amplitude of the oscillations, A_0, is determined by the pressure difference $\rho_l g\mathcal{F}L$ equal to 7.8 kPa for $\mathcal{F} = 0.97$, and 5.9 kPa for $\mathcal{F} = 0.73$. In both

configurations, the period of the oscillations decreases with time. With the spring-mass system analogy in mind, this evolution is a direct consequence of the reduction of mass of the water column along the emptying process, the volume of the top air buffer remaining constant.

The results of the numerical integration of Eqs. (3) and (6) are superimposed with the experimental data in Fig. 6. Experimental data are reported in blue symbols. Let us look first at the model predictions when a damping rate is imposed equal to zero, which are reported in black thin lines. The predictions then point out that the amplitude of the pressure fluctuations decreases for a part simply because the system loses energy via mass loss. For the case with $\mathcal{F} = 0.73$, this mainly reproduces the evolution of the amplitude. But for the case with $\mathcal{F} = 0.97$, additional dissipation of energy must definitively be considered to reproduce the experimental decrease of the pressure amplitudes. When optimizing the ability of the model to reproduce the experiments, the best-fitting parameters (α, β) are $(1.18, 170 \text{ N m}^{-3} \text{ s})$ and $(1.18, 1250 \text{ N m}^{-3} \text{ s})$, respectively, for $\mathcal{F} = 0.73$ and 0.97, indicating that the damping coefficient is indeed larger for the case with $\mathcal{F} = 0.97$. Figure 6 shows that the model including dissipation correctly reproduces the experimental results. Both the values of the extrema and the periodicity are well predicted by the model up to $t/\tau \approx 0.85$. Beyond this limit, the distance of the bubble nose to the upper free surface gets smaller than the cylinder diameter and the nose shape, and the free-surface deformations become strongly coupled, which has an important impact on their dynamics. Indeed, for $\mathcal{F} = 0.97$, as the bubble approaches the surface, we observed a flattening of the bubble nose associated with a rapid decrease of its mean rise speed. Concurrently, for $\mathcal{F} = 0.73$, the free surface exhibits sloshing and large deformations that can lead to the generation of a thin liquid jet expelled from the liquid bulk, as in [24]. The sloshing also influences the shape of the nose of the

bubble and, as a consequence, its velocity. The proximity of the bubble nose and of the free surface thus leads to strong nonlinear interactions that are not considered by the present simple mechanical model.

For the six experimental cases we explored, the best parameters (α, β) have been computed. The value of the polytropic coefficient is found to be independent of d^* and of $\mathcal{F}$, which vary, respectively, in the ranges [0.8 − 1] and [0.73 − 0.97]. Its value, equal to 1.17 ± 0.03, is consistent with previous findings [3] and indicates that the pressure evolution in the top air buffer thus stands in between an isothermal and an isentropic evolution. The value of the damping coefficient is also found to be independent of d^* but strongly dependent on the initial filling ratio, with $\beta_{0.97} = 1250 \pm 170$ N m^{-3} s for $\mathcal{F} = 0.97$ and $\beta_{0.73} = 170 \pm 30$ N m^{-3} s for $\mathcal{F} = 0.73$.

The fairly good agreement of the damped variable mass oscillator model with our experimental data is illustrated in Fig. 7. The results of the model are obtained with a constant damping coefficient equal to 1250 N m^{-3} s for $\mathcal{F} = 0.97$ and 170 N m^{-3} s for $\mathcal{F} = 0.73$ and a constant polytropic coefficient $\alpha = 1.17$. The time-dependent period, given by Eq. (9), matches well the time between the successive maxima of the recorded pressure signal for all the opening diameters and initial filling ratios that were investigated [Fig. 7(a)]. The period does not depend at all on the neck diameter. As predicted by Eq. (9), due to the unique value of α, the period is completely determined by the liquid outflow rate and $\mathcal{F}$, which fix, together with the polytropic coefficient, the spring constant $\sqrt{a}$ of the oscillator. As can be seen in Fig. 7(b), the amplitude of successive maxima of the pressure oscillations is also well predicted by the model [Eq. (9)]. It is found that the decay of the amplitude depends essentially on $\mathcal{F}$ and barely on d^*. For $\mathcal{F} = 0.73$ we obtain $\gamma = 0.69$, and for $\mathcal{F} = 0.97$ we obtain $\gamma = 2.62$. The concavity of $A(t)$ changes with the value of γ, in agreement with the model in which the evolution of the envelope of the amplitude is concave if $\gamma > 1$ and convex if $\gamma < 1$, as can be deduced from Eq. (9). From the definition of γ, it appears that $b\tau/2\rho_l$ is equal to 0.44 and 2.37 for $\mathcal{F} = 0.73$ and 0.97, respectively. It is worthwhile to note that in the case $\mathcal{F} = 0.73$, the energy loss is thus dominated by the loss of potential energy due to exiting mass, while it is dominated by the damping term when the cylinder is initially almost completely filled with water.

As previously mentioned, the deviation of the model from the data, observed for $t/\tau > 0.85$ when $d^* = 0.9$ or 1, is due to the proximity of the bubble nose with the free surface. But for $d^* = 0.8$, larger deviations are observed even at lower values of t/τ. These cases involve Taylor bubbles trailing a swarm of coalescing bubbles of moderate sizes. During its rising, the large bubble is no longer attached to the neck of the cylinder. For $\mathcal{F} = 0.73$, the model underestimates the period because at any time it underestimates the mass of liquid present in the cylinder. Indeed, the model propagates the gas phase at the tail of the Taylor bubble as if it was a full cylinder of gas while liquid is still present in the trailing swarm of bubbles. Similarly, for the case in which $\mathcal{F} = 0.97$ and $d^* = 0.8$, beyond $t/\tau = 0.7$, the experiments present more data scattering than for $d^* = 0.9$ or 1.
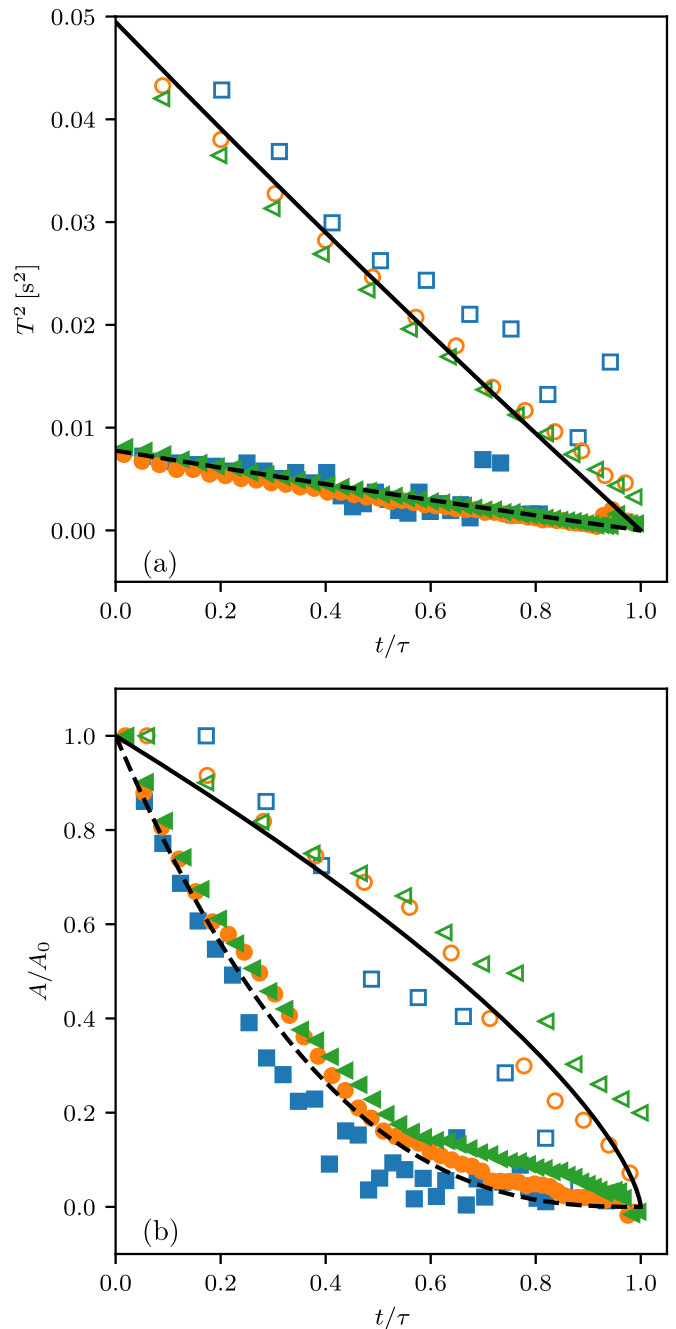

FIG. 7. Variation of (a) the amplitude and (b) the period of the pressure oscillations as a function of time. The symbols represent the experimental data obtained from the successive maxima of the oscillations for different diameter of the holes and initial fillings: □, $d^* = 0.8$; ○, $d^* = 0.9$; ◁, $d^* = 1$. Empty symbol, $\mathcal{F} = 0.73$; filled symbol, $\mathcal{F} = 0.97$; the solid and dashed lines represent the prediction of the model, Eq. (9), with $\beta_{0.97} = 1250$ N m^{-3} s, $\beta_{0.73} = 170$ N m^{-3} s, and $\alpha = 1.17$.

The physical origin of the damping is still unclear. In the present model, damping term has been chosen linear with respect to velocity. This is an *a priori* choice that allows a specific decrease of the pressure amplitude. While dissipation appears quite clearly as being the viscous dissipation associated with head losses in necks consisting in long tubes

[1], it has never been evaluated for an emptying with a thin-wall neck. If we analyze the possible causes of dissipation in the present system, we shall consider different physical processes.

The first one is viscous dissipation in the core of the flow and along the walls. Using a URANS model, numerical simulations of oscillating Taylor bubbles provided by Ambrose *et al.* [14] have shown that Stokes boundary layers are generated at the wall by the oscillatory bubble motion. Even if outside of the Stokes region the fluid behaves like a plug, a periodic viscous shear stress is, however, exerted at the walls. We can estimate an order of magnitude of the damping parameter β associated with the viscous force in the oscillatory boundary layer if we consider that the Stokes layer is present not only in the liquid region in front of the bubble nose, but also in the film surrounding the bubble. Indeed, the thickness of the falling film of liquid around the Taylor bubble can be estimated to be $0.04D \sim 4 \times 10^{-3}$ m [25], and it will always be larger than the Stokes layer width that varies during the emptying but in limited ranges for $t/\tau \leqslant 0.8$. Equation (9) (as well as Fig. 7) indicates that T decreases in the range 0.22–0.1 s for $\mathcal{F} = 0.73$ and in between 0.09 and 0.04 s for $\mathcal{F} = 0.97$. The Stokes layer thickness δ_{St} is thus always lower than the film one.

In the momentum conservation equation [Eq. (4)], a term representing a periodic viscous stress, denoted $\tilde{\tau}_w$, due to the presence of this Stokes layer would appear as $4\tilde{\tau}_w \mathcal{F}L/D$ if we assume that it is exerted all over the inner surface of the tube, along the total length $L_0 = \mathcal{F}L$. This oscillatory shear stress is different from the quasistationary one linked to the mean velocity present in particular in the thin liquid film, and it is due to the oscillating velocity $\dot{\delta z}$. As in [14], $\tilde{\tau}_w$ can be approximated from its amplitude $\tilde{\tau}_w \approx -\rho \nu_l \dot{\delta z}/\delta_{St}$. This provides $\beta \approx 4\rho \nu_l L_0/(\delta_{St}D)$. This expression of β proves to be independent of d^* and to increase with $\mathcal{F}$ as observed

in the experiments. It leads for $\mathcal{F} = 0.73$ and 0.97 to values that are in the respective ranges $[128 - 192]$ and $[268 - 451]\,\mathrm{N\,m^{-3}\,s}$ when ω varies during the emptying. Although the value obtained for the case $\mathcal{F} = 0.73$ agrees well with the experimental data, the value of β for the largest value of $\mathcal{F}$ is less satisfactory, indicating that additional dissipative processes are affecting the dynamics.

Other sources of dissipation can be found in the singular pressure loss at the neck of the cylinder as in [24], in the sloshing motion of the upper free surface as in [26], or in the heat exchange during the successive compressions of the top air buffer [27]. The deformability of the bubble can also damp the pressure oscillation by converting part of the corresponding energy into interfacial energy of gas-liquid interfaces [3]. Modeling of such dissipation terms is not easy at all and is beyond the scope of this contribution. However, this study shows that a viscous damping, proportional to the velocity, with a constant damping coefficient, is able to accurately represent the dissipative processes. Viscous dissipation in the Stokes layer appears to be a dominant contribution compatible with the dependency on the initial filling ratio. The connection of the damping term introduced in Eq. (4) to viscous dissipation is not inconsistent with the inviscid fluid assumption made in Sec. IV B to analyze the flow around the nose of the rising bubble. While viscosity is essential, at least to dissipate the continuously decreasing gravitational potential energy of the liquid phase, it is expected to have little effect on the bubble rise speed as long as the bubble Reynolds number remains sufficiently large. For the value reached in this study ($\mathrm{Re}_b \sim 10^4$), the flow near the front of the bubble, which is entirely dominated by inertia, can be studied under the restrictive assumption of an inviscid fluid. This point of view, adopted in the present study as well as in a large number of studies on Taylor bubbles [4–6,20,21], is supported, among others, by [28].
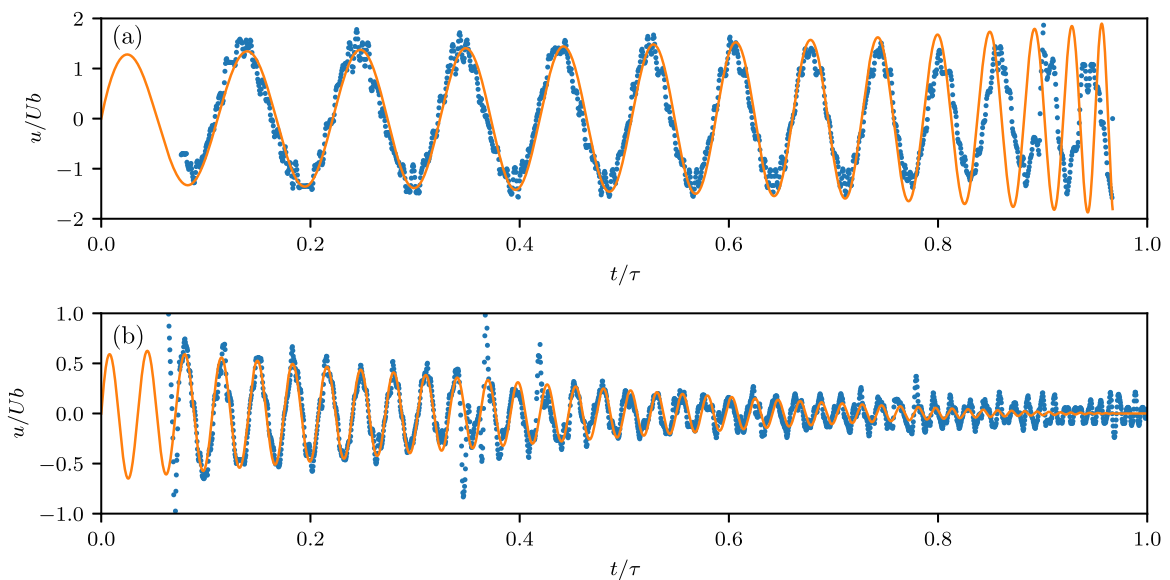

FIG. 8. Comparison of the time evolution of the velocity fluctuation of the apex between the prediction of the model and the experimental data for a full opening ($d^* = 1$) and two different initial filling ratios (a) $\mathcal{F} = 0.73$ and (b) $\mathcal{F} = 0.97$. The parameters (α, β) correspond to best-fitting values and are $(1.18, 170)$ for $\mathcal{F} = 0.73$ and $(1.14, 1250)$ for $\mathcal{F} = 0.97$.
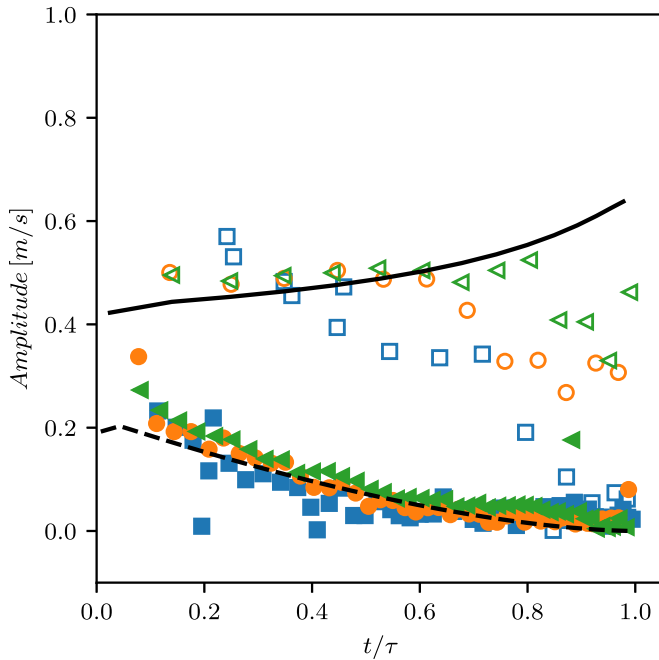
FIG. 9. Comparison of the time evolution of the amplitude of the oscillations of the velocity fluctuation of the apex between the prediction of the model and the experimental data for different diameters of the hole and initial fillings: $\square$, $d^* = 0.8$; $\bigcirc$, $d^* = 0.9$; $\triangleleft$, $d^* = 1$. Empty symbol, $\mathcal{F} = 0.73$; filled symbol, $\mathcal{F} = 0.97$; the solid and dashed lines represent the model with $\beta_{0.97} = 1250$, $\beta_{0.73} = 170$, and $\alpha_0 = 1.17$.

B. Apex velocity model versus experiments

The coupling between the free-surface motion and the rise speed of the bubble nose is described by Eq. (15). This equation is numerically integrated with the free-surface velocity $u_{fz} = \dot{\delta z}$ coming from the integration of Eq. (6). The fairly good agreement of the prediction of the model with the experimental data is illustrated in Fig. 8 for the same two cases as those presented in Fig. 6. For each configuration, it is found that both the amplitude and the period of appearance of the successive maxima are well predicted up to $t/\tau = 0.7$–0.8. It was previously mentioned that the model fails to accurately predict the pressure beyond such a value, and this contributes to the discrepancies observed in the prediction of the apex velocity. In addition, as the bubble nose approaches the free surface, the velocity potential defined by Eq. (10) is no longer a solution due to the change in the boundary conditions. Figure 9 shows that up to $t/\tau = 0.7$–0.8, the prediction of the amplitudes of the velocity fluctuations is satisfactory for most of the cases. The clear deviation observed for $d^* = 0.8$ and $\mathcal{F} = 0.73$ is related to the fact that the Taylor bubble there is detached from the neck of the cylinder and trails a swarm of smaller bubbles. The model of temporal evolution of the liquid mass involved in the pressure oscillations model is then less pertinent. Indeed, already in Fig. 7 the case at $d^* = 0.8$ and $\mathcal{F} = 0.73$ showed deviations between predictions and experimental measurement of the pressure oscillations. Because the motion of the free surface that excites the Taylor bubble oscillations is poorly predicted, the amplitudes of the bubble velocity oscillations cannot be satisfactorily predicted for this case.

VI. CONCLUSION

This study spotlights a new feature of the flow resulting from the emptying of a vertical cylindrical bottle initially filled with water that is observed for large aperture ($d^* \geqslant 0.8$) and when the cylinder is only partially filled. The flow is then characterized by a long Taylor bubble that invades the cylinder at a speed that periodically oscillates in time. This motion is coupled to vertical oscillations of the position of the free surface limiting the top air buffer around an equilibrium value that remains unchanged along the emptying.

We have proposed a physical model where the pressure of the top air buffer and thus the free-surface position is represented by a variable mass oscillator. The period is determined by the compressibility of the top air buffer while the amplitude of the pressure oscillations decreases under the conjugate effects of mass loss and dissipative processes. The motion of the bubble is solved assuming that the unsteady flow generated by the free-surface motion is potential in the vicinity of the apex of the bubble.

The good agreement between the prediction of the model and the experimental data suggests that the dissipative processes are well modeled by a viscous damping with a constant damping coefficient that depends essentially on the initial filling ratio. This description is consistent with the existence of oscillating boundary layers, but it is also able to represent the effect of other dissipative processes that affect the dynamics. However, it would be interesting to perform additional experiments, either with fluids of different viscosities, or with other initial filling ratios, to assess how well the Stokes boundary layer can describe the viscous dissipation. In this complex flow, it would also be interesting to analyze how the response of the thickness of the thin liquid film surrounding the Taylor bubble is coupled to these oscillations. Indeed, while our field of view did not allow us to measure its thickness, it was nevertheless possible to oversee that surface waves with similar periods propagate along the film.

ACKNOWLEDGMENTS

[1] A. A. K. Tehrani, M. A. Patrick, and A. A. Wragg, Dynamic fluid flow behaviour of a tank draining through a vertical tube, Int. J. Multiphase Flow **18**, 977 (1992).

[2] C. Clanet and G. Searby, On the glug-glug of ideal bottles, J. Fluid Mech. **510**, 145 (1999).

[3] S. Mer, O. Praud, J. Magnaudet, and V. Roig, Emptying of a bottle: How a robust pressure-driven oscillator coexists with

complex two-phase flow dynamics, Int. J. Multiphase Flow **118**, 23 (2019).

[4] D. T. Dumitrescu, Stromung an einer luftblase im senkrechten rohr, Z. Angew. Math. Mech. **23**, 139 (1943).

[5] R. M. Davies and G. I. Taylor, The mechanics of large bubbles rising through extended liquids and through liquids in tubes, Proc. R. Soc. Ser. A **200**, 375 (1950).

[6] C. Clanet, P. Héraud, and G. Searby, On the motion of bubbles in vertical tubes of arbitrary cross-sections: Some complements to the Dumitrescu-Taylor problem, J. Fluid Mech. **519**, 359 (1999).

[7] P. B. Whalley, Flooding slugging and bottle emptying, Int. J. Multiphase Flow **13**, 723 (1987).

[8] P. B. Whalley, Two-phase flow during filling and emptying of bottles, Int. J. Multiphase Flow **17**, 145 (1991).

[9] O. Schmidt and J. Kubie, An experimental investigation of outflow of liquids from single-outlet vessels, Int. J. Multiphase Flow **21**, 1163 (1995).

[10] S. S. Kordestani and J. Kubie, Outflow of liquids from single-outlet vessels, Int. J. Multiphase Flow **22**, 1023 (1996).

[11] S. Tang and J. Kubie, Further investigation of flow in single inlet/outlet vessels, Int. J. Multiphase Flow **23**, 809 (1997).

[12] R. Dougall and M. Kathiresan, Dynamic behavior of fluid flow through a vertical tube into a sealed tank filled with gas, Chem. Eng. Commun. **8**, 289 (1981).

[13] C. C. Pringle, S. Ambrose, B. J. Azzopardi, and A. C. Rust, The existence and behaviour of large diameter Taylor bubbles, Int. J. Multiphase Flow **72**, 318 (2015).

[14] S. Ambrose, D. Hargreaves, and I. Lowndes, Numerical modeling of oscillating Taylor bubbles, Eng. Appl. Computat. Fluid Mech. **10**, 578 (2016).

[15] D. Brannock and J. Kubie, Velocity of long bubbles in oscillating vertical pipes, Int. J. Multiphase Flow **22**, 1031 (1996).

[16] S. Madani, O. Caballina, and M. Souhar, Unsteady dynamics of Taylor bubble rising in vertical oscillating tubes, Int. J. Multiphase Flow **35**, 363 (2009).

[17] S. Madani, O. Caballina, and M. Souhar, Some investigations on the mean and fluctuating velocities of an oscillating Taylor bubble, Nucl. Eng. Des. **252**, 135 (2012).

[18] S. Mer, O. Praud, H. Neau, N. Merigoux, J. Magnaudet, and V. Roig, The emptying of a bottle as a test case for assessing interfacial momentum exchange models for Euler-Euler simulations of multi-scale gas-liquid flows, Int. J. Multiphase Flow **106**, 109 (2018).

[19] J. Flores, G. Solovey, and S. Gil, Variable mass oscillator, Am. J. Phys. **71**, 721 (2003).

[20] R. Collins, F. De Moraes, J. Davidson, and D. Harrison, The motion of a large gas bubble rising through liquid flowing in a tube, J. Fluid Mech. **89**, 497 (1978).

[21] X. Lu and A. Prosperetti, Axial stability of Taylor bubbles, J. Fluid Mech. **568**, 173 (2006).

[22] E. White and R. Beardmore, The velocity of rise of single cylindrical air bubbles through liquids contained in vertical tubes, Chem. Eng. Sci. **17**, 351 (1962).

[23] D. Layzer, On the instability of superposed fluids in a gravitational field, Astrophys. J. **122**, 1 (1955).

[24] É. Lorenceau, D. Quéré, J.-Y. Ollitrault, and C. Clanet, Gravitational oscillations of a liquid column in a pipe, Phys. Fluids **14**, 1985 (2002).

[25] E. Llewellin, E. Del Bello, J. Taddeucci, P. Scarlato, and S. Lane, The thickness of the falling film of liquid around a Taylor bubble, Proc. R. Soc. A **468**, 1041 (2012).

[26] S. Marrone, A. Colagrossi, F. Gambioli, and L. González-Gutiérrez, Numerical study on the dissipation mechanisms in sloshing flows induced by violent and high-frequency accelerations. I. theoretical formulation and numerical investigation, Phys. Rev. Fluids **6**, 114801 (2021).

[27] H. N. Oguz and A. Prosperetti, The natural frequency of oscillation of gas bubbles in tubes, J. Acoust. Soc. Am. **103**, 3301 (1998).

[28] J. Fabre and A. Liné, Modeling of two-phase slug flow, Annu. Rev. Fluid Mech. **24**, 21 (1992).